INTERNATIONAL JOURNAL FOR NUMERICAL METHODS IN FLUIDS
Int. J. Numer. Meth. Fluids **31**: 703–720 (1999)

CALCULATION OF THREE-DIMENSIONAL TURBULENT FLOW WITH A FINITE VOLUME MULTIGRID METHOD

C. CORNELIUS, W. VOLGMANN* AND H. STOFF

Lehrstuhl fur Fluidenergiemaschinen, Ruhr-Universitat Bochum, 44780 Bochum, Germany

SUMMARY

A numerical method for the efficient calculation of three-dimensional incompressible turbulent flow in curvilinear co-ordinates is presented. The mathematical model consists of the Reynolds averaged Navier–Stokes equations and the k–ε turbulence model. The numerical method is based on the SIMPLE pressure-correction algorithm with finite volume discretization in curvilinear co-ordinates. To accelerate the convergence of the solution method a full approximation scheme-full multigrid (FAS-FMG) method is utilized. The solution of the k–ε transport equations is embedded in the multigrid iteration. The improved convergence characteristic of the multigrid method is demonstrated by means of several calculations of three-dimensional flow cases. Copyright © 1999 John Wiley & Sons, Ltd.

KEY WORDS: finite volume method; Navier–Stokes equations; multigrid method; turbulent flow; three-dimensional curvilinear co-ordinates

1. INTRODUCTION

The application of CFD methods in engineering problems shows that for sufficient accuracy the mesh resolution has to be reasonably high. Unfortunately, conventional single-grid Navier–Stokes solvers suffer from poor convergence characteristics, in particular on relatively fine grids. The computational effort varies nearly with the square of the number of grid point. This leads quickly to unacceptable large computing times for complex flow problems. Hence, there is an increasing demand on more efficient solution methods.

The applications of multigrid methods to solve elliptic PDEs iteratively have shown nearly optimum convergence characteristics, i.e. the computation times are directly proportional to the number of grid points. These considerations have lead to the development of multigrid methods for the Navier–Stokes equations.

Recent works, which are based on the SIMPLE pressure correction scheme, mostly deal with laminar flow (Becker *et al.* [1], Smith and Vanka [2], Orth and Schönung [3]). Depending on the complexity of the discretized geometry, speed-ups of two orders of magnitude for two-dimensional cases are reported compared with single-grid method. The methods of Lien and Leschziner [4], Rubini *et al.* [5] and Peric *et al.* [6] are able to handle turbulent flows by use of a k–ε turbulence model, but they are restricted to two-dimensional geometries and orthogonal grids respectively. Further, Nowak *et al.* [7] extend the coupled solution strategy of Vanka [8] to a multigrid algorithm for laminar flow cases. Another approach, that of Sheng [9], is based on the pseudo-compressibility method of Chorin [10].

* Correspondence to: Lehrstuhl fur Fluidenergiemaschinen, Ruhr-Universitat Bochum, 44780 Bochum, Germany.

CCC 0271–2091/99/200703–18$17.50

Received March 1998
Revised July 1998

This paper describes a finite volume multigrid method (FAS-FMG) for the calculation of turbulent flows in complex three-dimensional geometries. Results are shown for the lid-driven laminar flow in a cavity and turbulent flow cases of different complexities. Special emphasis lies on the analysis of the performance of the multigrid method compared with the standard single-grid method.

2. GOVERNING EQUATIONS

The mathematical model consists of the Reynolds averaged Navier–Stokes equations and the standard k–ε turbulence model. Formulated for Cartesian velocity components and co-ordinates, the conservation equations are:

Continuity equation:

$$\frac{\partial c_i}{\partial x_i} = 0. \tag{1}$$

Momentum equation:

$$\frac{\mathrm{D}c_i}{\mathrm{D}t} = -\frac{1}{\rho}\frac{\partial(\delta_{i,j}p)}{\partial x_j} + \frac{\partial}{\partial x_j}\left((v_\mathrm{t}+v)\left(\frac{\partial c_i}{\partial x_j}+\frac{\partial c_j}{\partial x_i}\right)\right). \tag{2}$$

Transport of the turbulent kinetic energy:

$$\frac{\mathrm{D}k}{\mathrm{D}t} = \frac{1}{\sigma_k}\frac{\partial}{\partial x_j}\left(v_\mathrm{t}\frac{\partial k}{\partial x_j}\right) + \frac{\partial c_l}{\partial x_j}v_\mathrm{t}\left(\frac{\partial c_l}{\partial x_j}+\frac{\partial c_j}{\partial x_l}\right) - \varepsilon. \tag{3}$$

Transport of the dissipation rate of the turbulent kinetic energy:

$$\frac{\mathrm{D}\varepsilon}{\mathrm{D}t} = \frac{1}{\sigma_\varepsilon}\frac{\partial}{\partial x_j}\left(v_\mathrm{t}\frac{\partial \varepsilon}{\partial x_j}\right) + \frac{\partial c_l}{\partial x_j}v_\mathrm{t}\left(\frac{\partial c_l}{\partial x_j}+\frac{\partial c_j}{\partial x_l}\right)c_{1\varepsilon}\frac{\varepsilon}{k} - c_{2\varepsilon}\frac{\varepsilon^2}{k}. \tag{4}$$

Kolmogorov–Prandtl relation:

$$v_\mathrm{t} = c_\mu\frac{k^2}{\varepsilon}, \tag{5}$$

with i, j and l ranging from 1 to 3 for the three Cartesian components.

3. NUMERICAL PROCEDURE

The discretization is based on a collocated finite volume arrangement with Cartesian velocity components in which all variables are located at the cell centers. Second-order discretization schemes are used for the diffusion terms of the transport equations. For the convection terms, flux blending [11] and higher-order upwind schemes, such as QUICK [12] and MUSCL [13], have been employed. The calculation of the cell face mass fluxes is done according to the momentum interpolation of Rhie and Chow [14] to avoid oscillations of the variables.

The momentum, continuity and turbulence equations are solved in a decoupled manner. So the discretization procedure leads to a set of linearized systems of algebraic equations for each conservation equation of the following form:

$$\sum_m a_m \Phi_m = S_{\Phi P}, \tag{6}$$

where Φ_m are the values for a 7-point discretization stencil, respectively in matrix form:

$$[A(\vec{\Phi})]\vec{\Phi} = \vec{S}(\vec{\Phi}). \tag{7}$$

These systems of equations are solved sequentially with modified version of Stones strongly implicit procedure (SIP) [15]. The fields of pressure and velocity are coupled according to the SIMPLE algorithm of Patankar and Spalding [16]. Firstly, the momentum equations are assembled and solved by treating the fields of pressure, mass fluxes and turbulence quantities as known. Secondly, the modified continuity equation is used to calculate pressure correction values so that the velocity field satisfies mass conservation. With the updated variables, the equations of the turbulence model are treated. Convergence is achieved when the normalized sums of absolute residuals are fallen below a prescribed value. The convergence criteria used here range from 10^{-4} to 10^{-5}. This means an accuracy to approximately 4–5 significant figures of the solution. Details of the discretization process are described by Greim [17].

4. MULTIGRID METHOD

The conventional iterative single-grid methods for solving the Navier–Stokes equations, like the widespread SIMPLE-based or pseudo-compressibility methods, suffer from poor convergence characteristics on very fine grids. These algorithms possess the so-called smoothing property: the solver removes only the high frequency, short wavelength Fourier components of the error. The low frequency components, which have a long wavelength compared with the grid spacing, are damped weakly. The solver seems to focus only on local residuals. Unfortunately, on increasingly fine grids, the portion of the low frequency error components increases and the solution becomes more tenacious. This phenomenon was discovered in the field of iterative numerical solutions of algebraic equations arising from discretizing elliptic partial differential equations. Brandt first suggests the use of several grid levels to accelerate the solution process [18]. The aim of the multigrid method is to efficiently damp the longwave error components, which are remaining on the fine-grid, on successively coarsened grids. The error, which was smoothed on the fine grid, is transferred to the coarser grids without loss of information. Here again the iterative smoother is applied. The calculated coarse-grid error components are summed up and prolongated to the fine-grid level.

The efficiency of this procedure is based on two facts: first, the smoothing property causes that the restricted error field, which appears as high frequency on the coarse grid, is damped much faster on the coarse grid than on the fine grid; secondly, the numerical effort on the coarse grid is much smaller. In three-dimensional problems, the required work is reduced to about one eighth per coarsening level.

For a single non-linear system of equations like (7) the multigrid method can be written as follows. The application of v sweeps of an iterative solver to the system (7) leads to an approximate solution Φ^v, which satisfies the residual equation:

$$R^v = \vec{S}(\vec{\Phi}^v) - [A(\vec{\Phi}^v)]\vec{\Phi}^v. \tag{8}$$

Combining Equations (7) and (8) and the transfer to the coarse grid (superscript H) leads to the fundamental coarse grid full approximation scheme (FAS) equation:

$$[A^{\mathrm{H}}(\vec{\tilde{\Phi}}^{\mathrm{H}})]\vec{\tilde{\Phi}}^{\mathrm{H}} = \vec{S}^{\mathrm{H}}(\vec{\Phi}^{\mathrm{H}}) + \{I_h^{\mathrm{H}}\vec{R}^{vh} - \vec{S}^{\mathrm{H}}(I_h^{\mathrm{H}}\vec{\Phi}^{vh}) + [A^{\mathrm{H}}(I_h^{\mathrm{H}}\vec{\Phi}^{vh})]I_h^{\mathrm{H}}\vec{\Phi}^{v}\}, \tag{9}$$

with the definition of the full approximation $\vec{\hat{\Phi}}$,

$$\vec{\hat{\Phi}}^{\mathrm{H}} = I_h^{\mathrm{H}} \vec{\Phi}^{vh} + \Delta \vec{\Phi}^{\mathrm{H}}, \tag{10}$$

and the restriction transfer operator I_h^{H} of the variables from fine to coarse grids.

The assembling of the coarse grid equation (9) in the described way assures that, for vanishing fine grid residuals $\vec{R}^{vh}$, no corrections $\Delta\vec{\Phi}^{\mathrm{H}}$ for the fine-grid values are calculated. The term inside the braces depends only on the restricted fine-grid values. Hence, it is not changed during the coarse-grid iteration and represents the influence of the fine-grid smoothing process. By the use of the full approximation variable it is possible to take into account the dependence of the matrix $[A]$ and the source term $\vec{S}$ of $\hat{\Phi}$ on the coarse grids. The updated fine-grid variables are calculated as

$$\vec{\hat{\Phi}}^{vh}_{\mathrm{new}} = \vec{\Phi}^{vh}_{\mathrm{old}} + I_{\mathrm{H}}^{h}(\vec{\hat{\Phi}}^{\mathrm{H}} - I_h^{\mathrm{H}} \vec{\Phi}^{vh}), \tag{11}$$

where the bracket term represents the fine-grid correction according to Equation (10).

In the case of the SIMPLE algorithm there are some special features of the multigrid procedure that arise from the coupling between pressure and velocity fields. The discretized fine-grid momentum equations with separated pressure terms read:

$$\sum a_m^h c_{im}^h = -(b_i^1 \partial p^1 + b_i^2 \partial p^2 + b_i^3 \partial p^3)_P^h + S_{iP}^h(c_i^h). \tag{12}$$

An analogous procedure, as demonstrated for a single system of equations, yields the coarse-grid equation

$$\sum a_m^{\mathrm{H}} \hat{c}_{im}^{\mathrm{H}} = -(b_i^1 \partial p'^1 + b_i^2 \partial p'^2 + b_i^3 \partial p'^3)_P^{\mathrm{H}} + S_{iP}^{\mathrm{H}}(\hat{c}_{iP}^{\mathrm{H}}) + \left\{ I_h^{\mathrm{H}} R_{c_i}^{vh} - S_{iP}^{\mathrm{H}}(I_h^{\mathrm{H}} c_{iP}^{vh}) + \sum a_m^{vh}(I_h^{\mathrm{H}} c_{im}^{vh}) \right\}, \tag{13}$$

where $\hat{c}_i^{\mathrm{H}}$ stands for the full approximation of the Cartesian velocity components on the coarse grids. The operator of the pressure terms in (12) is linear, hence, in the coarse grid, equations appear as pressure corrections rather then full approximations of the pressure. So the coarse-grid pressure correction algorithm works on corrections of corrections. The treatment of the coarse-grid mass fluxes is an important issue of the multigrid procedure. To get a consistent formulation without mass imbalance between the different grid levels, the coarse-grid fluxes are calculated based on the restricted fine-grid fluxes. The flux corrections are evaluated based on the velocity corrections, which are calculated on the coarse grid.

Sivaloganathan has shown for a simplified case, that the SIMPLE algorithm possesses the smoothing property so that the efficient use in a multigrid procedure is possible [19].

In the case of turbulent flow calculation it is essential for the multigrid performance that the transport equations of the k–ε model are embedded in the coarse-grid iteration. Otherwise only weak speed-ups can be achieved.

The 2-grid multigrid cycle explained above can be applied recursively through sequences of grid levels. There are different strategies to control the intergrid transfer. First, the transfer may depend on dynamic criteria like residual reduction rate. This means that, if the convergence rate on the current grid level is too low, the restriction to the next coarser grid is performed. Secondly, the grid change can be initiated following prescribed numbers of iteration sweeps. In this study, a fixed V-cycle (Figure 1) is used for changing the different grid levels. The numbers of pre- and post-smoothing relaxation sweeps are prescribed. Standard values are from four to six sweeps for the restriction and from one to four sweeps for the

prolongation process. In this manner, the optimum compromise between convergence characteristics and generality is achieved. Other cycle forms are possible, of which some work better in certain cases.

An updating correction of the fine-grid values is suppressed in the case of a diverging coarse-grid solution. This arrangement is especially necessary at the initial iteration for the calculation of complex turbulent flow problems.

For optimal convergence characteristics, a full multigrid (FMG)-cycle, as shown in Figure 2, has been adopted. The iteration procedure starts on the coarsest grid. After some relaxation sweeps the solution is prolongated to the next finer grid to be used as an initial approximation.

Then a V-cycle is initiated on this level. The procedure is repeated consecutively until the finest grid level is reached, where conventional multigrid V-cycle begins. The test calculation showed up to two orders of magnitude residual reduction from this FMG-cycle at a computational effort of only five to ten fine-grid sweeps. In the case of turbulent flow, calculations the fields of k and ε are interpolated to the next finer grid, the fine-grid values of the turbulent viscosity ν_t are calculated according to Equation (5).

For the finite volume discretization, the coarse grids are built up by standard coarsening, eight fine-grid control volumes are put together to one coarse-grid control volume. For the prolongation of the correction values to the fine grids and the restriction to the coarse grids, a trilinear interpolation method is utilized. For the simplified two-dimensional case, Figures 3 and 4 illustrate the interpolation schemes for regular control volumes.

As mentioned above, the transfer of the fine-grid residues and fluxes is done by conservative summation, as shown schematically by the arrows in Figure 3.

Next to the coarse-grid pressure correction, the correct implementation of the coarse-grid boundary conditions is crucial for convergence and efficiency of the multigrid procedure, especially the treatment of the turbulence quantities, which requires particular attention.

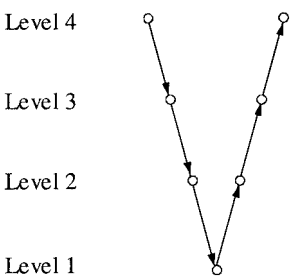

Figure 1. V-cycle.

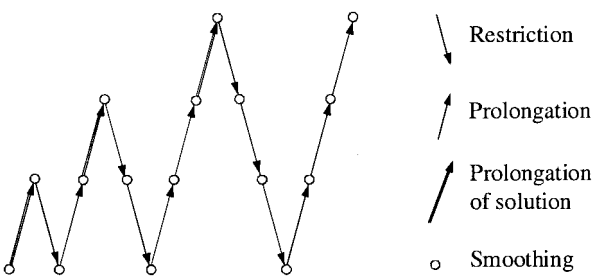

Figure 2. FMG-cycle.

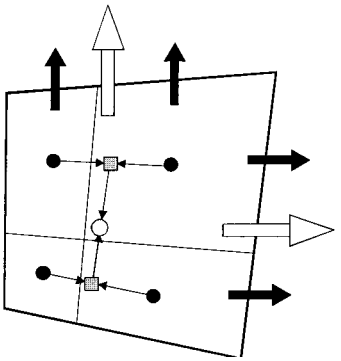

Figure 3. Restriction: ●, fine-grid cv-centre; ○, coarse-grid cv-centre.

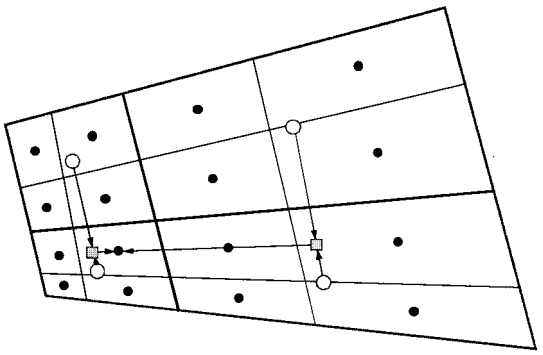

Figure 4. Prolongation: ●, fine-grid cv-centre; ○, coarse-grid cv-centre.

The coarse-grid boundary conditions for the velocities are the same as on the fine-grid, except at the outlet boundary, where on the fine-grid a gradient condition is applied. The velocity values at this boundary are not changed during coarse-grid iteration. After the interpolation to the coarse-grid the velocity values are corrected once to achieve consistent calculation of the coarse-grid mass fluxes. Thereafter, the velocities and the restricted outlet mass fluxes are held constant. On walls the velocities are zero, this is set in the same way on the coarse grids. Hence, according to Equation (10), no corrections of the fine-grid values are calculated.

For the k and ε equations, the fine-grid values at wall-adjacent cells are calculated with wall functions. The application of wall functions to the coarse grids would lead to unphysical values because of the great wall distance of the cell centers. So the restricted boundary values of k and ε are held constant, and hence no corrections are calculated. To satisfy the realizability constraint, the restricted turbulence properties and prolongated correction values are modified. So destabilizing negative values of these variables are avoided.

For efficient storage, a data structure of one-dimensional arrays for all variables of the three-dimensional calculation domain has been chosen. The different grid levels are arranged, one after the other, in these arrays. Pointers are used to get the initial and final index for each grid level. Figure 5 shows this arrangement for a data structure with three grid levels. A second effect of this storage method is a nearly optimum vectorization level of 98–99%, because of the one-dimensional structure of the calculation loops.

Furthermore, this technique leads to an easy handling of the different grid levels in the various subroutines. The storage requirement of the multigrid code is about 20% above the single-grid code.

5. APPLICATIONS

The following section presents some of the calculation examples carried out with the described method. Priority lies on the analyses of the multigrid performance compared with the original single-grid code. Validation against experimental data is less comprehensive, because this is done for the single-grid code in the work of Greim [17]. For each calculation it is assured that there are no differences (in the limits of numerical accuracy) between multigrid and single-grid solutions. The examples are shown with increasing complexity, beginning with a simulation for the lid-driven laminar flow in a cavity to prove the successful implementation of the basic multigrid procedure. After the presentation of the calculation of the turbulent flow in a rectangular 90° bend, the results for the turbulent flow in an S-shaped diffusor and the flow over two wall-mounted hemispheres in a duct are shown.

5.1. Lid-driven laminar flow in a cavity

Numerous calculations have been performed for the cubic lid-driven cavity. Computational results are presented here for a grid consisting of 274625 points and a Reynolds number $Re = c_{\text{lid}}/b/v$ of 100. Figure 6 shows the grids of the 4-level calculation.

Figure 7 shows the typical helical streamline pattern inside the cavity, calculated from the solution field. Fluid is transported away from the symmetry plane to the outer walls along the side faces. In the center of the main vortex, the fluid flows back to the symmetry plane of the cavity.

A comparison of the multigrid and the single-grid solutions is made by examining the relative differences of each variable. The maximum difference of the velocity magnitude between the 3-level FMG and the single-grid solution is 0.00014%. This very small value is a result of the low convergence criterion of 10^{-5} for the normalized residuals, which is used for this example. Therefore, multigrid and single-grid methods give the same results only limited by the accuracy of the iteration.

For comparison of the convergence rates, Figure 8 shows the normalized c_1-momentum residuals of the single-grid, the 2-level, 3-level and the 4-level FMG procedure plotted against the fine-grid iteration number. The residual plots presented in this paper shows always that the residual component that is decisive for the convergence of the calculation. To reach the convergence tolerance of 10^{-5}, the 4-level calculation requires 45 and the single-grid calculation 1544 fine-grid iterations. The small value of the convergence tolerance is prescribed to prove the correct convergence of the coarse-grid algorithm.

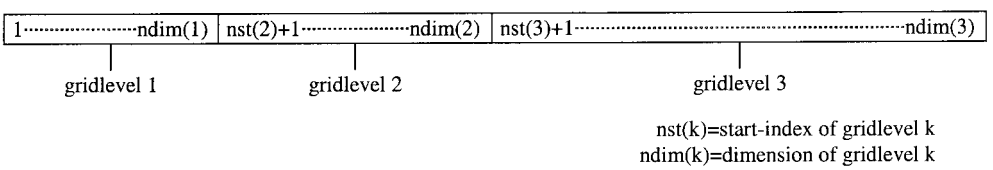

Figure 5. One-dimensional array for three grid levels.

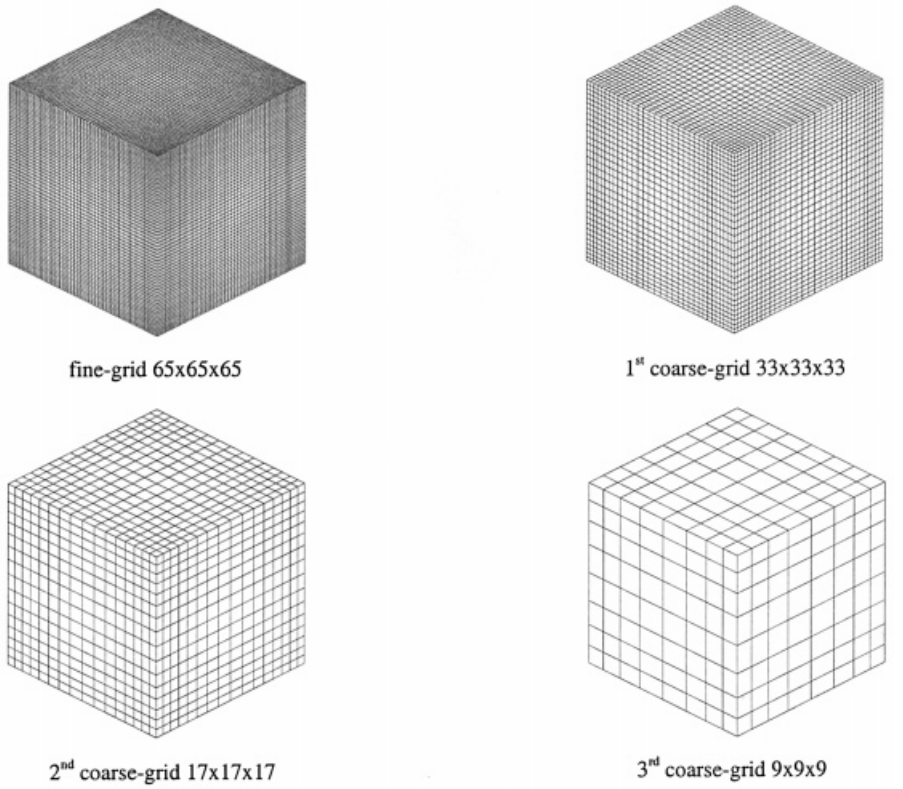

Figure 6. Grids for 4-level calculation of lid-driven cavity.

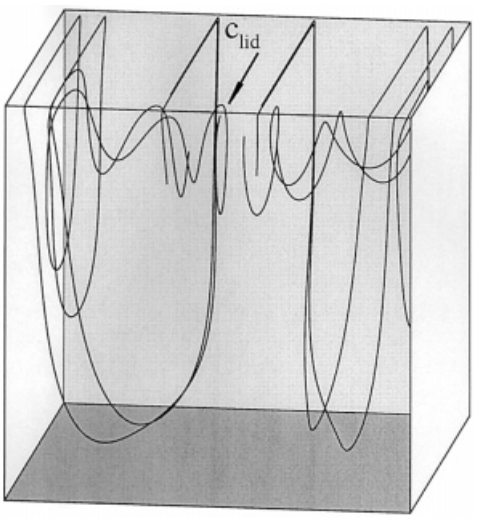

Figure 7. Streamlines of the flow inside the cavity.

Table I summarizes the main computational features of the test calculation. The computations were performed on a Siemens/Fujitsu VPP300/8 vectorcomputer. Two things are essential: first, there is a dramatic reduction in the number of fine-grid iterations (work units, WU). The speed-up factor between the single-grid and the 4-level FMG in the case of the WU is almost 35. The reduction of the residuals of five orders of magnitude requires only 45 fine-grid iterations for 274625 grid points compared with more than 1500 iterations for the conventional single-grid method. Secondly, there is a constant increasing ratio between the speed-up in WU and the speed-up in CPU time. This is a result of the increasing effort that is done on the higher number of coarse grid levels.

To conclude, the results show the successful implementation of the basic multigrid algorithm as the speed-up ratios are comparable with those presented in the literature [20].

5.2. Turbulent flow in a rectangular bend

The geometry of this example is described in detail by Kim *et al.* along with extensive experimental data [21]. The Reynolds number $Re = u_\infty H/v$ is $Re = 224000$, where the height H is the smallest extension of the cross-section. Figure 9 shows the grids of the 3-level calculation. The fine-grid consists of $121 \times 25 \times 73$ respectively 220825 grid points.

Extensive comparisons between measured and calculated flow fields were carried out. As an example, Figure 10 displays the normalized streamwise velocity component u^* in a plane at 45° angle of the 90° bend for two discretization schemes of the convective fluxes (first-order

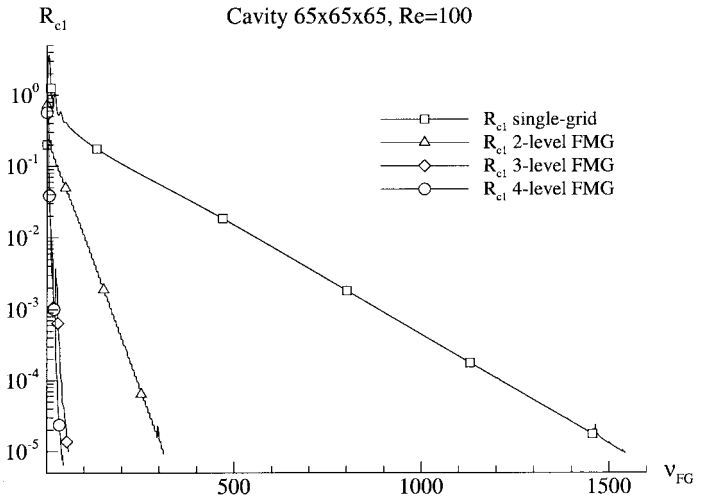

Figure 8. Convergence history for the lid-driven cavity.

Table I. Convergence features for the lid-driven cavity flow

Method	CPU time [s] VPP300	WU	Speed-up CPU	Speed-up WU
Single-grid	956.3	1544	1	1
2-Level FMG	239.7	313	3.99	4.93
3-Level FMG	49.6	59	19.28	26.17
4-Level FMG	39.0	45	24.52	34.31

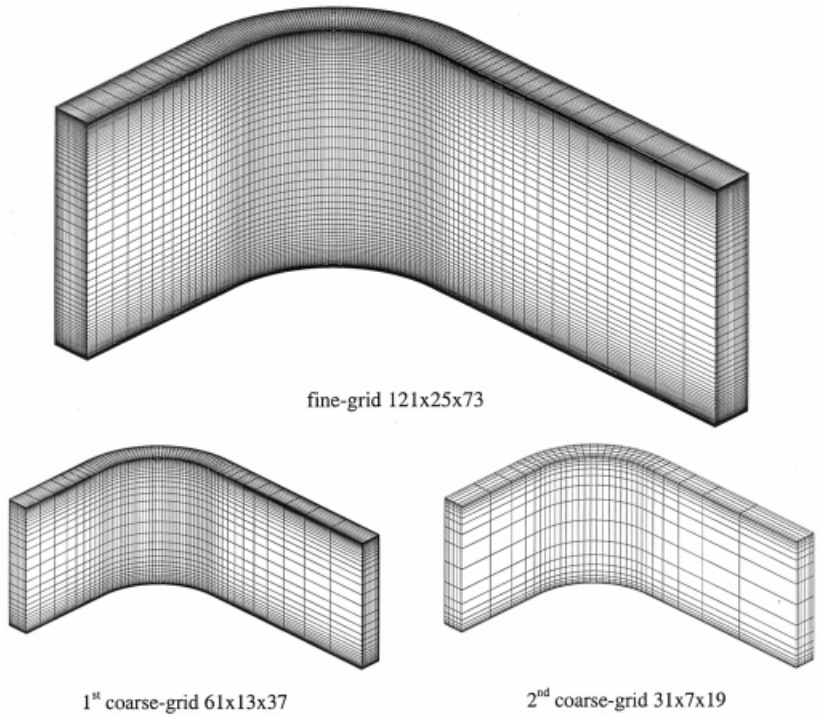

Figure 9. Grids for 3-level calculation of rectangular bend flow.

upwind and higher-order MUSCL) and the measurement. The different levels, decreasing from the outer ($y^* = 6\%$) to the inner ($y^* = 94\%$) radius of the bend, correspond well to the experimental data. The MUSCL scheme resolves the regions of steeper gradients slightly better than the first-order upwind scheme.

The same variable is plotted in Figure 11, now at 75° angle of the 90° bend. Again the prediction of the velocity levels is reasonably good and the upwind scheme underpredicts the local minima at $y^* = 6\%$ due to the larger numerical diffusion.

The convergence histories for the different solution schemes are shown in Figure 12. The additional reduction of the fine-grid iteration number is remarkable, if in the case of the 3-level calculation the FMG-cycle is used. The saving in CPU time is about 44 s, which is more than 40% of the total CPU time.

The calculations are carried out on a VPP300 vectorcomputer, the corresponding values of CPU times and work units for the different solution methods are presented in Table II.

5.3. 3D turbulent flow in an S-shaped diffusor

A detailed geometric description of the test case is given by Peric [11]. The grids of the computational domain for the 3-level calculation are shown in Figure 13. The fine-grid consists of 290 521 grid points. The Reynolds number is $Re = c_{\text{in}} b/\nu = 40\,000$, with the width b at the square inlet of the diffusor and c_{in} the mean velocity at the inlet.

Figure 14 displays the calculated pressure contours in several cross-sections and in the symmetry plane. The prediction shows the typical two extreme at the bottom side of the diffusor. As a result of the fluid deceleration, a maximum is located at the end of the first

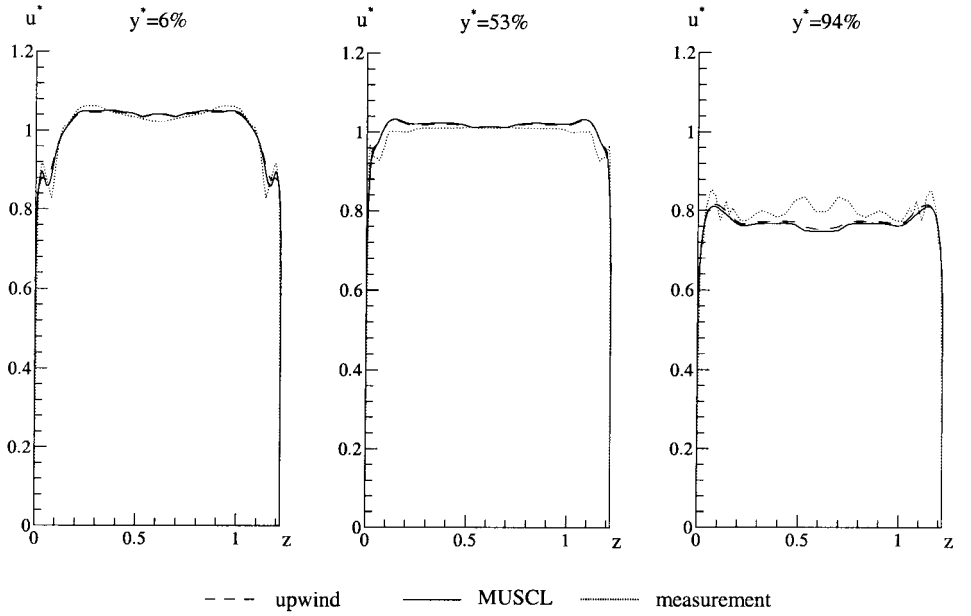

Figure 10. Streamwise velocity component u^* at 45° angle of the 90° bend.

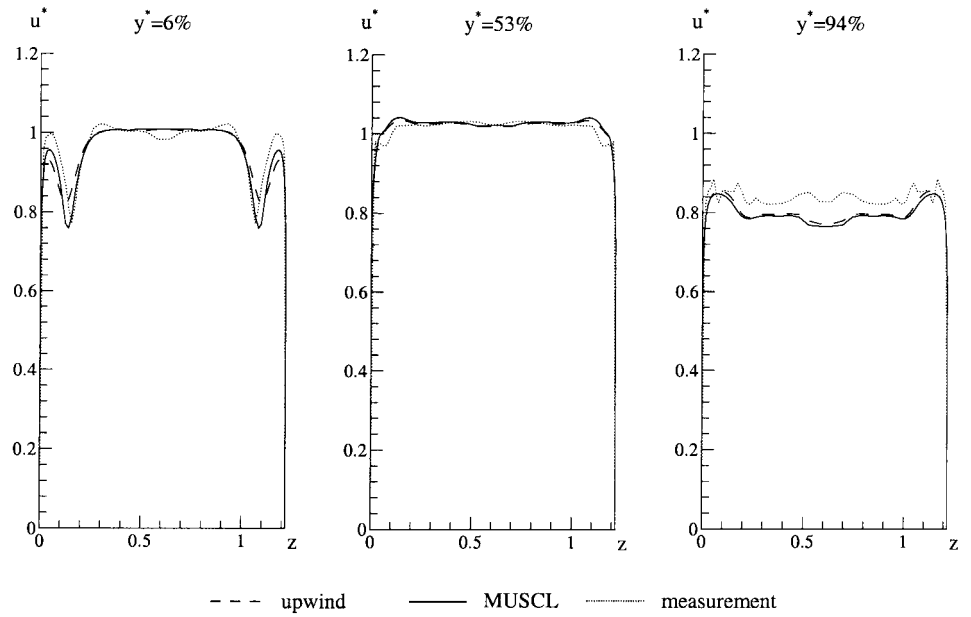

Figure 11. Streamwise velocity component u^* at 75° angle of the 90° bend.

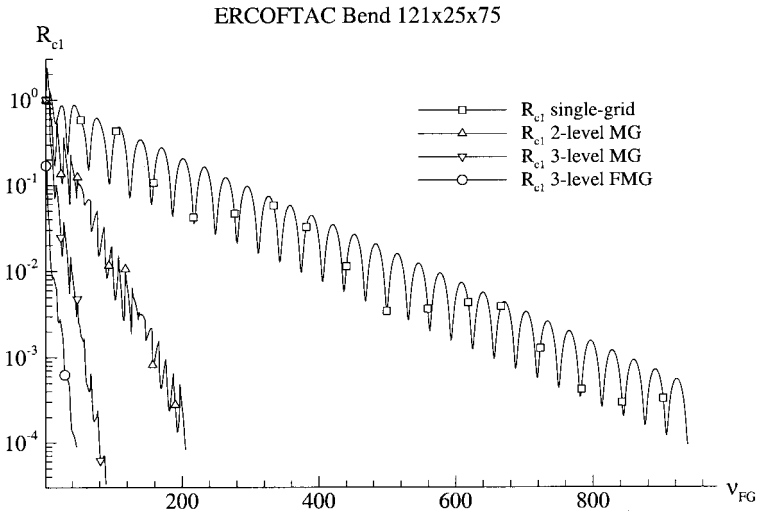

Figure 12. Convergence history for the rectangular bend flow.

Table II. Convergence features for the rectangular bend flow

Method	CPU time [s] VPP300	WU	Speed-up CPU	Speed-up WU
Single-grid	953.7	938	1	1
2-Level MG	250.1	205	3.81	4.58
3-Level MG	101.7	89	9.38	10.54
3-Level FMG	57.7	46	16.53	20.39

bend, close to the change in the curvature. The minimum immediately follows the flow entering the second bend. The nearly constant pressure in the cross-section between the two bends is remarkable.

Figure 15 illustrates the convergence rates by the normalized residuals of the velocity component c_1 for the single-grid, the 2-level and the 3-level FMG procedure.

The single-grid method did not converge very well, so the relaxation parameters, especially α_p have to be reduced. This leads to a rather high number of the fine-grid iterations. Similar observations are made by Peric [11]. The reduction of the initial fine-grid residues due to the use of the FMG-cycle is evident. In the case of the 3-level calculation, the reduction is more than one order of magnitude. The 2-level FMG scheme obtains no residual reduction because the initial calculation on the first coarse grid (with high values of the relaxation parameters) converges even worse than the fine grid calculation.

The calculations are again carried out on a single processor of a VPP300/8 vectorparallel-computer. The corresponding values of the computational performance for the various solution methods are presented in Table III.

The computation time is reduced from more than 26 min to less than 3 min. Again, the 3-level FMG-cycle leads to an additional saving in the computation time of approximately 30% compared with the conventional 3-level MG-procedure.

5.4. Turbulent flow around two wall-mounted hemispheres

The geometry of this test case consists of a duct with rectangular cross-section and two hemispheres mounted on opposite walls of the duct. The calculation domain together with

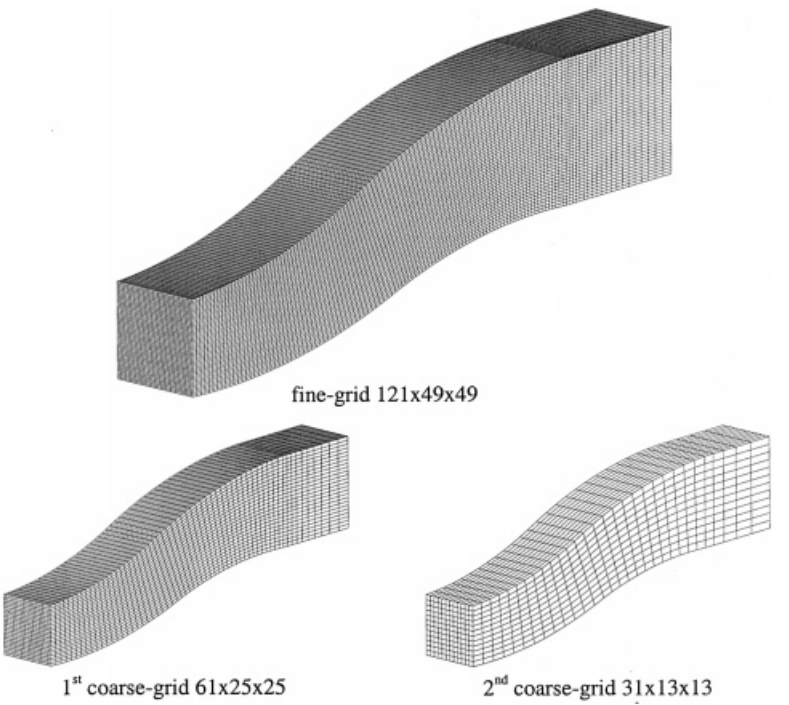

Figure 13. Grids for 3-level calculation of S-shaped diffusor flow.

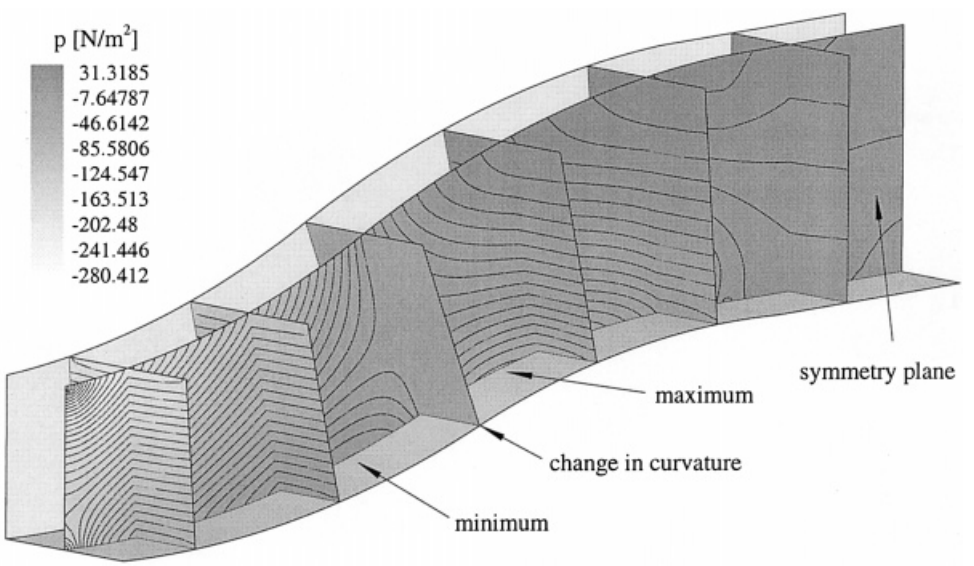

Figure 14. Calculated pressure contours in the S-shaped diffusor.

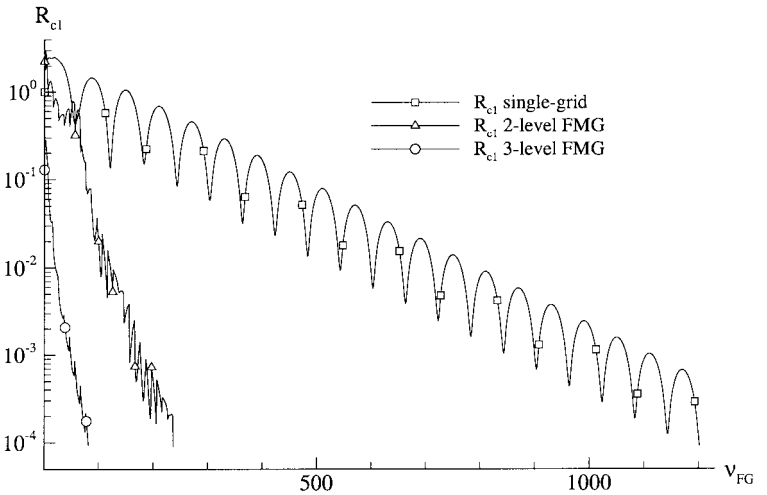

Figure 15. Convergence history for the S-shaped diffusor flow.

Table III. Convergence features for the S-shaped diffusor flow

Method	CPU time [s] VPP300	WU	Speed-up CPU	Speed-up WU
Single-grid	1583.1	1202	1	1
2-Level FMG	398.2	237	3.98	5.07
3-Level FMG	173.7	82	9.11	14.66

details of the grids for the 3-level calculation are shown in Figure 16, viewed in streamwise direction. The fine-grid consists of 321 681 mesh points. The Reynolds number $Re = c_{in}d/v$ is 20 000, with d the diameter of the spheres and c_{in} the mean velocity at the inlet of the duct.

This test case includes severe mesh skewness and high aspect ratios to analyse the performance of the multigrid method under these conditions. In particular the junction between the duct surfaces and the border of the hemispheres leads to extremely distorted cells. The skew angles in this region are less than 10° on the finest grid.

Figure 17 shows the calculated streamlines close to the surface of the hemisphere viewed onto the top of the sphere. A symmetric vortex pair is formed in the separation region behind the sphere.

The secondary velocity vectors viewed in streamwise direction in the center plane of the spheres are plotted in Figure 18. A secondary motion from the convergent region between the two spheres into the unthrottled cross-section of the duct is generated.

Figure 19 presents the convergence histories of the single-grid, the 2-level and the 3-level FMG method.

The use of a second coarse grid (3-level FMG calculation) only slightly improves the convergence rate. The additional effort for the second coarse grid does not pay off, because the saving in fine-grid iterations remains moderate. So the 2- and 3-level calculation reach about the same speed-up in computation time, as shown in Table IV.

Despite considerable mesh skewness, the multigrid method leads to a reduction from 412 to 151 fine-grid iterations to reach the prescribed convergence criterion of 10^{-4}. Nevertheless, the

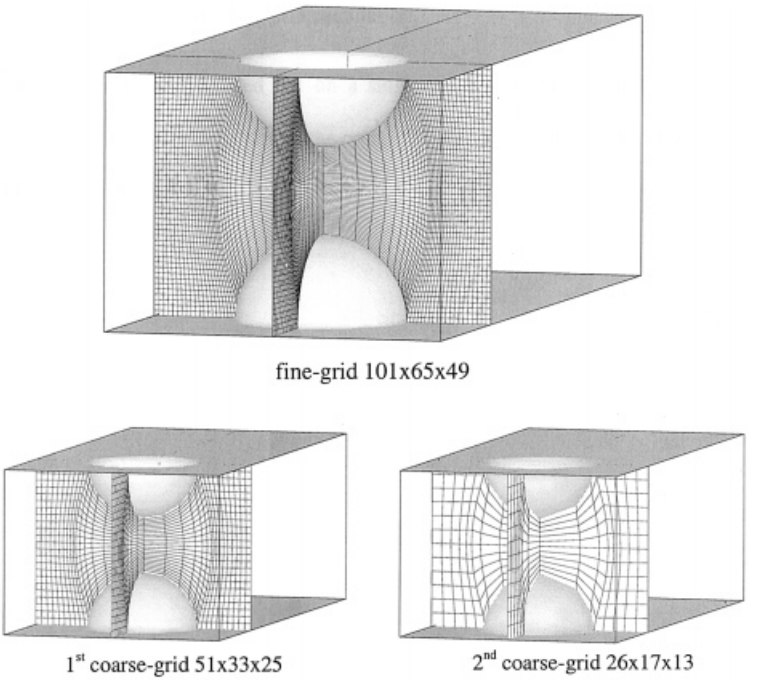

Figure 16. Grids for 3-level calculation of the flow around two hemispheres.

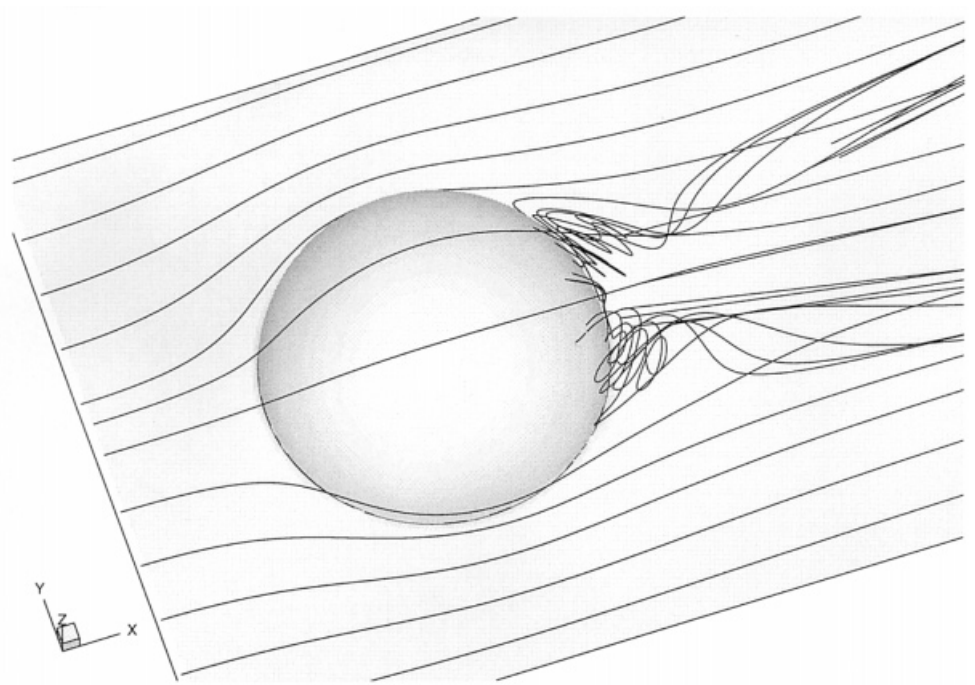

Figure 17. Streamlines of the flow around one of the two hemispheres.

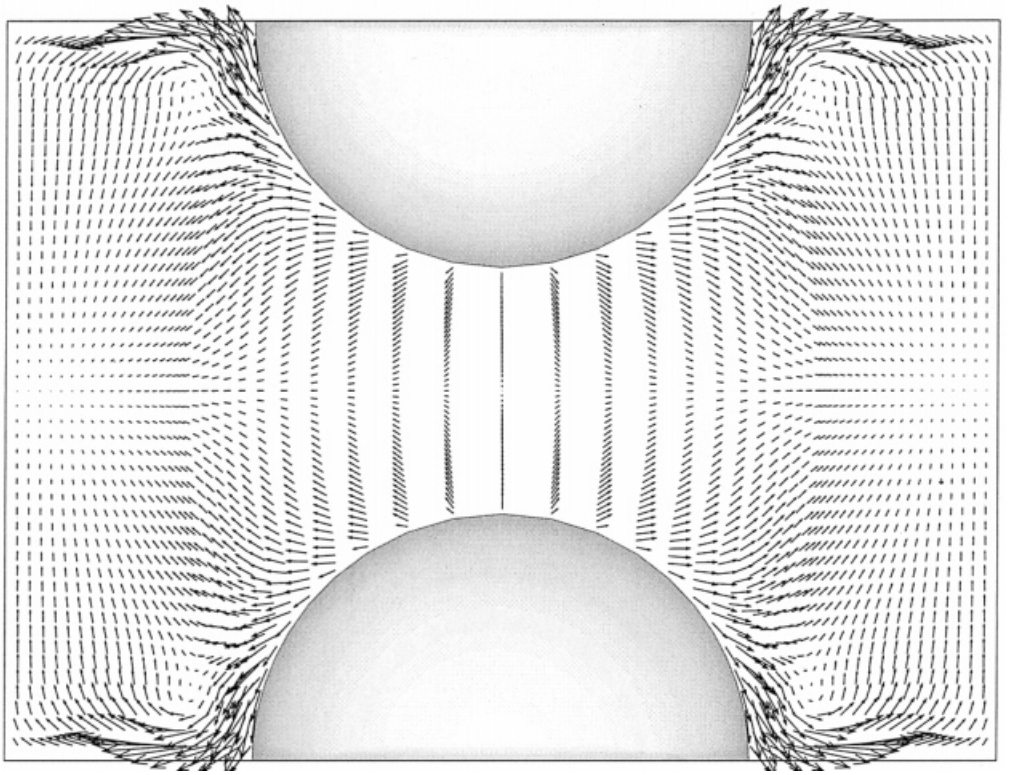

Figure 18. Secondary velocity vectors in cross-section.

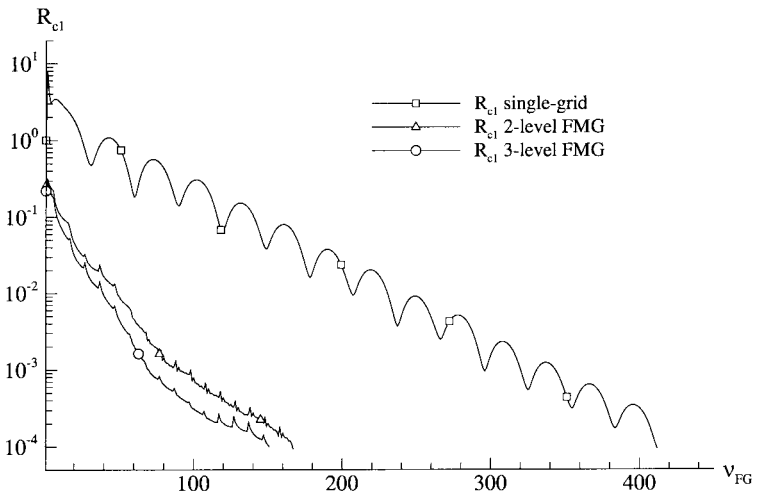

Figure 19. Convergence history for the hemisphere flow.

Table IV. Convergence features for the flow around two hemispheres

Method	CPU time [s] VPP300	WU	Speed-up CPU	Speed-up WU
Single-grid	606.8	412	1	1
2-Level FMG	323.0	167	1.88	2.47
3-Level FMG	306.7	151	1.98	2.73

savings are significantly less than in the test cases mentioned previously. The main reason is the poor mesh quality. In the case of strong non-orthogonality, the bilinear interpolation functions are less accurate. Furthermore, the convergence rate of the single-grid method reaches nearly optimum values with four orders of magnitude reduction in residuals on 321 685 grid points in only 412 fine grid iterations.

6. CONCLUSIONS

The main features of an FAS-FMG method for the Reynolds averaged Navier–Stokes equations have been presented. The performed test calculations demonstrate the potential of the multigrid technique for improving the convergence not only in simple geometric configurations but also in complex, turbulent flow cases. The multigrid method shows speed-ups in the CPU time ranging from 2 to 16 times for turbulent flow cases, depending on the mesh size and grid complexity. For more elliptical laminar flows of low Reynolds numbers the FAS-FMG method indicates nearly optimum convergence characteristics. The multigrid performance can deteriorate at higher Reynolds numbers, poor mesh quality and complex boundary conditions, but it is especially superior on high dense grids. Considering the increasing computer memory capabilities the future use of CFD methods will permit the use of high number of mesh points. Hence, the multigrid method is an appropriate approach to get solutions for these fine grids in acceptable run times. Future developments concern the extension of the method to the application to incompressible turbomachinery flow.

ACKNOWLEDGMENTS

The work reported herein was supported by the Deutsche Forschungsgemeinschaft under grant Sto $328/1+2$, for which the authors wish to express their gratitude. The calculations were performed on the Siemens/Fujitsu VPP 300 vectorcomputer at the Computing Center of the RWTH Aachen.

REFERENCES

1. C. Becker, H.J. Ferziger, M. Peric and G. Scheuerer, 'Finite volume multigrid solution of the two-dimensional, incompressible Navier–Stokes equations', *Notes Numer. Methods Fluids*, **23**, 37–47 (1988).
2. K.M. Smith, W.K. Cope, S.P. Vanka, 'A multigrid procedure for three-dimensional flows in non-orthogonal collocated grids', *Int. J. Numer. Methods Fluids*, **17**, 887–904 (1993).
3. A. Orth and B. Schönung, 'Calculation of 3D laminar flows with complex boundaries using a multigrid method', *Notes Numer. Methods Fluids*, **28**, 446–453 (1990).
4. F.S. Lien and M.A. Leschziner, 'Multigrid convergence acceleration for complex flow including turbulence', in W. Hackbusch, U. Trottenberg (eds.), *Multigrid Methods III*, *International Series on Numerical Mathematics*, vol. 98, Birkhauser, Basel, 1991, pp. 277–288.

5. P. Rubini, H. Becker, E. Grandmaison, A. Pollard, A. Sobiesak and C. Thurgood, 'Multigrid acceleration of three-dimensional, turbulent, variable-density flows', *Numer. Heat Transf. Part B*, **22**, 163–177 (1992).
6. M. Peric, M. Ruger and G. Scheuerer, 'A finite volume multigrid for calculating turbulent flows', *Proc. 7th Symp. on Turbulent Shear Flows*, Stanford University, 1989.
7. Z.P. Nowak and M. Salcudean, 'Turbulent flow calculations by the non-linear multigrid method', *Z. Angew. Math. Mech.*, **76**, 463–469 (1996).
8. S.P. Vanka, 'Block-implicit calculation of steady turbulent recirculating flows', *Int. J. Heat Mass Transf.*, **28**, 2093–2103 (1985).
9. C. Sheng, L.K. Taylor and D.L. Whitfield, 'Multigrid algorithm for three-dimensional incompressible high-Reynolds number turbulent flows', *AIAA J.*, **33**, 2073–2079 (1995).
10. A.J. Chorin, 'A numerical method for solving incompressible viscous flow problems', *J. Comput. Phys.*, **2**, 12–26 (1967).
11. M. Peric, 'A finite volume method for the prediction of three-dimensional fluid flow in complex ducts', *Ph.D. Thesis*, University of London, 1985.
12. B.P. Leonard, 'A stable and accurate convective modeling procedure based on quadratic upwind interpolation', *Comput. Methods Appl. Mech. Eng.*, **19**, 59–67 (1979).
13. B. van Leer, 'Towards the ultimate conservative difference scheme V. A second sequel to Godunov's method', *J. Comput. Phys.*, **32**, 101–136 (1979).
14. C.M. Rhie and W.L. Chow, 'Numerical study of the turbulent flow past an airfoil with trailing edge separation', *AAIA J.*, **21**, 1525–1532 (1979).
15. H.-J. Leister and M. Peric, 'Vectorized strongly implicit solving procedure for seven-diagonal coefficient matrix', *Int. J. Numer. Methods Heat Fluid Flow*, **4**, 159–172 (1994).
16. S.V. Patankar and D.B. Spalding, 'A calculation procedure for heat, mass and momentum transfer in three-dimensional parabolic flows', *Int. J. Heat Mass Transf.*, **15**, 1787–1806 (1972).
17. R. Greim, 'Entwicklung eines Finite-Volumen-Verfahrens zur Berechnung dreidimensionaler, reibungsbehafteter, inkompressibler, instationärer Strömungen in einer Turbomaschinenstufe beliebiger Bauart', *Dissertation*, Ruhr-Universitat Bochum, 1995.
18. A. Brandt, 'Multigrid techniques, a guide with applications to fluid dynamics', *GMD-Studien*, *No. 85*, 1984.
19. S. Sivaloganathan and G.J. Shaw, 'On the smoothing properties of the SIMPLE pressure correction algorithm', *Int. J. Numer. Methods Fluids*, **8**, 441–461 (1988).
20. Z. Lilek, S. Muzaferija and M. Peric, 'Efficiency and accuracy aspects of a full-multigrid simple algorithm for three-dimensional flows', *Numer. Heat Transf. Part B*, **31**, 23–42 (1997).
21. W.J. Kim and V.C. Patel, 'Origin and decay of longitudinal vortices in developing flow in a curved duct', *J. Fluids Eng.*, **116**, 45–52 (1994).

